Available online at www.sciencedirect.com

SciVerse ScienceDirect

Ceramics International 38 (2012) 6469–6480

CERAMICS INTERNATIONAL

www.elsevier.com/locate/ceramint

Effect of ball milling on reactive spark plasma sintering of B_4C–TiB_2 composites

L. Nikzad[a,b], R. Licheri[a], T. Ebadzadeh[b], R. Orrù[a,*], G. Cao[a]

[a]*Dipartimento di Ingegneria Meccanica, Chimica e dei Materiali, Unità di Ricerca del Consorzio Interuniversitario Nazionale per la Scienza e Tecnologia dei Materiali (INSTM), Unità di Ricerca del Consiglio Nazionale delle Ricerche (CNR), Dipartimento di Energia e Trasporti—University of Cagliari, Piazza D'Armi, 09123 Cagliari, Italy*

[b]*Division of Nanotechnology and Advanced Materials, Materials and Energy Research Center, P.O. Box 14155-4777, Tehran, Iran*

Received 6 February 2012; received in revised form 9 May 2012; accepted 9 May 2012
Available online 17 May 2012

Abstract

The influence of mechanical activation by ball milling (BM) of Ti, B and graphite powders mixture on the synthesis of dense B_4C-41% vol. TiB_2 composite by Spark Plasma Sintering (SPS) is investigated. BM treatment produces grains size refinement (50–150 nm) in the processing powders and the formation of TiB and TiB_2, when milling times are longer than 6 h.

The synthesis process occurs through a solid-state diffusion mechanism where the first crystalline phase formed is TiB, which is gradually converted to TiB_2, while the formation of B_4C takes place subsequently. The complete conversion of unmilled reactants is reached at about 1500 °C, while this goal is achieved at 1100 °C when using 3 h milled powders. A near to fully dense product with fine grained microstructure (down to submicrometer level) and homogeneous phases distribution is obtained by SPS when starting from 8 h milled powders, if the applied current intensity does not overcome 1150 A.

Keywords: A. Milling; D. Borides; D. Carbides; Spark Plasma Sintering

1. Introduction

Due to the combination of its remarkable hardness, high melting temperature, low density, wear resistance, chemical stability, neutron absorption capability, etc., boron carbide is a very attractive material in several innovative and traditional industrial fields, particularly for neutron absorption, armor, thermoelectric and cutting tools applications [1]. In spite of these interesting properties, the diffusion of this ceramic is hindered due to its intrinsic brittleness and the difficulties encountered when sintering the corresponding powders for the fabrication of massive bodies.

Therefore, a considerable effort has been devoted in the last two decades to the improvement of B_4C sintering behavior and mechanical properties. In this context, the introduction of appropriate amounts of a suitable reinforcing phase, particularly TiB_2, to the B_4C matrix is well known to produce a useful contribution to overcome both drawbacks mentioned above [1].

Thus, several bulk ceramic composites in the B_4C–TiB_2 system have been investigated by various researchers using different fabricating routes [2–21].

So far, the majority of the investigations took advantage of the conventional pressureless (PLS) [2,5,8,9,12,14,15] or hot-pressing (HP) [3,4,6,10,11,18] techniques, although alternative approaches, such as high-pressure sintering [7], hot-isostatic pressing (HIP) [5], crucibleless zone melting method [16], plasma pressure compaction (P^2C) [13], and pulsed electric current sintering (PECS) [17,19–21] have been also adopted.

Regardless the sintering method utilized, the obtainment of bulk B_4C–TiB_2 composites has been addressed either starting directly from the previously synthesized ceramic constituents in powder form [2,4–7,12–16,21] or after accomplishing the reaction synthesis and densification in a single step using appropriate reaction promoters [3,8,9,11,17–20].

*Corresponding author. Tel.: +39 70 6755076; fax: +39 70 6755057.
E-mail address: orru@dicm.unica.it (R. Orrù).

0272-8842/$36.00
http://dx.doi.org/10.1016/j.ceramint.2012.05.024

Most of the reactive sintering methods make use of B_4C and TiO_2 (with or without additional C) reactants [8,9,11,18–20] according to the general synthesis reaction $(1+x)B_4C+2xTiO_2+3xC \rightarrow B_4C+2xTiB_2+4xCO$. Alternatively, B_4C and TiC ($B_4C+2TiC \rightarrow 2TiB_2+3C$) [3] or elemental titanium, boron and carbon black ($Ti+10B+2C \rightarrow 2B_4C+TiB_2$) [17] are also used as powder reagents.

Due to the covalent nature of boron carbide and titanium diboride bonds, temperature levels equal or above 2100 °C are required for achieving adequate densification levels during pressureless sintering of B_4C/TiB_2 composites [2,8,9,12,14,15]. On the other hand, relatively milder temperature conditions are needed when an external pressure is simultaneously applied, as for the case of conventional HP [6,10,11,18] or PECS [17,19–21] methods. The latter one, often indicated as Spark Plasma Sintering (SPS), is a relatively novel technology where the powders and the die containing them are crossed by a pulsed electric current and simultaneously subjected to a mechanical pressure [22]. It is well established that heating processes are strongly accelerated during SPS in contrast with the relatively long processing times (typically on the order of hours) encountered in conventional HP, where the energy required for sintering is provided by an external heating source. Furthermore, in comparison to HP, the higher heating rates and shorter dwell times obtained using SPS typically lead to materials with relatively finer microstructure, as a consequence of the more favorable sintering conditions which avoid excessive grain growth.

Along this direction, a positive contribution for promoting sintering phenomena and obtaining bulk $B_4C–TiB_2$ composite with homogeneous and fine microstructure was demonstrated to be provided by a mechanical treatment of the starting powders to be either only sintered [6] or simultaneously reacted and sintered [17]. In particular, B_4C-23% vol TiB_2 composite products with relative density higher than 95% were obtained by SPS at 1700 °C after 5 min holding time when using 16 h co-milled Ti, B, and C black powders [17]. In this study, the significant amount of WC detected in milled powders due to contamination from milling media was reported to lead to the presence of $(Ti,W)B_2$ in sintered samples.

In the present work, the fabrication of dense B_4C-41% vol TiB_2 composite by Reaction induced Spark Plasma Sintering (RSPS) starting from titanium, amorphous boron and graphite is addressed for the first time. Specifically, the effect of ball milling on the characteristics of powder reactants, SPS process behavior, reactants conversion, product relative density and microstructure is systematically investigated.

2. Experimental

Titanium (99.5% purity, particle size < 125 μm, Merck), amorphous boron (95–97% purity, particle size < 9 μm, Aldrich), and graphite (particle size < 20 μm, Aldrich) were used as raw materials. The relative content of each component in the mixture was calculated according to the following reaction:

$$Ti+6B+C \rightarrow B_4C+TiB_2 \quad (1)$$

Correspondingly, the reaction product consists of the TiB_2-59% vol B_4C composite, whose theoretical density (3.33 g/cm^3) was determined on the basis of a rule of mixture [23] which accounts for B_4C and TiB_2 densities, i.e. 2.5 and 4.5 g/cm^3 [24], respectively.

Mechanical activation of the starting mixture was carried out by co-milling reactants in a SPEX 8000 shaker mill (SPEX CertiPrep, USA) under Argon atmosphere, using stainless steel jars (65.8 cm^3 internal volume) and 4 stainless steel balls (10 mm diameter, 8 g weight). Milling runs included repeated cycles of 1 h of milling followed by 1 h cooling. The effect of milling time was investigated in the range 0–12 h while the ball to powder weight or charge ratio (CR) was maintained constant to 8.

Contamination of iron from milling media to processing powders was evaluated by means of ICP-OES (VISTA MPX-VARIAN).

Reactive sintering experiments were performed under vacuum conditions (20 Pa) using an SPS 515 S model equipment (Sumitomo Coal Mining Co. Ltd, Japan). The adopted pulse cycle consisted of 12 pulses on and 2 pulses off, for a total pulse cycle duration equal to 46.2 ms, with characteristic time of single pulse equal to about 3.3 ms.

About 2.5 g of powder mixture was poured inside a cylindrical graphite die (outside diameter, 30 mm, inside diameter, 15 mm, height, 30 mm). To protect the dies/plungers and make sample release easier after sintering, a graphite foil (0.13 mm thick, Alfa Aesar, Karlsuhe, Germany) was inserted between the internal surface of the die and the sample as well as between its top/bottom surface and the plungers. Heat losses by thermal radiation were limited by covering the die with a 2 mm thick layer of graphite felt (Atal s.r.l., Italy).

The SPS apparatus was used under current controlled mode, by increasing at a constant rate the integral mean electric current up to a maximum value in the range of 1100–1200 A during a time interval of 5 min (t_H) and then maintaining this current level (I) for additional 5 min (t_D). Nevertheless, the current application was interrupted at various time intervals $t_i \leq t_T = 10$ min when investigating the mechanism of formation of the $B_4C–TiB_2$ composite during reactive sintering. The mechanical pressure in all SPS experiments was held constant to 20 MPa.

Temperatures, applied current, voltage, and vertical displacement of the lower electrode (δ) were recorded in the real time. In particular, the measured displacement provides an indication of powder compact densification, although thermal expansion of the samples, electrodes, graphite blocks, spacers and plungers also contributes to this parameter [25].

Temperature measurements were carried out using a C-type thermocouple (Omega Engineering Inc., USA),

inserted in a small hole drilled on the lateral surface of the graphite die, as well as by means of a two-color pyrometer (Ircon Mirage OR 15–990, USA).

Samples density were measured by geometric and Archimedes method, using distilled water as a wetting liquid. For the sake of reproducibility, each experiment was repeated at least twice.

Phase identification of powders and sintered samples was carried out by XRD using a Philips PW 1830 X-rays diffractometer equipped with a Ni filtered Cu K_α radiation ($\lambda = 1.5405$ Å). Crystallite size of selected powdered samples was estimated by means of the Williamson and Hall method [26] from the line broadening of XRD peaks, where the two contributions to diffraction lines broadening, namely, the refinement of crystallite size and the internal strain, are both accounted for.

The microstructure and local phase composition of powders and bulk products were investigated by SEM (mod. S4000, Hitachi, Japan) and EDS analysis (Kevex Sigma 32 Probe, Noran Instruments, USA), respectively.

3. Results and discussion

3.1. Mechanical milling of reactants

The XRD patterns of the powder mixture as a function of the milling time at CR = 8 are reported in Fig. 1. All the major peaks appearing in the XRD spectra of unmilled powders correspond to Ti and C, although the presence of some crystalline boron in the commercial amorphous boron used in the present investigation is evidenced by the small peaks observed in the 15°–25° 2θ range. This feature is also revealed in similar studies recently reported in the literature where the same type of boron was employed as reactant [17]. It is seen from Fig. 1 that the original sharp graphite peak is significantly reduced after only 1 h milling and finally disappears in the XRD spectra relative to 3 h milled powders. Based on the results reported in the literature relatively to B–C and Ti–C binary systems [27–32], different explanations are possible to justify graphite peak disappearance by milling. For instance, the occurrence of such feature in Ti–C mixtures was ascribed to the localization of graphite within sandwiched Ti layers or in Ti grain boundaries, that makes C detection difficult, also because of the large differences in Ti and C mass absorption coefficients [27,28]. On the other hand, this outcome was also assigned to graphite amorphization phenomena [31]. More recently, the formation of transitional bonding states between C and Ti atoms was also postulated [32]. Moreover, the absence of graphite peaks after 2 h milling of B–C mixtures was considered a consequence of the dissolution of C atoms into B lattice to form supersaturated solid solutions [29].

Since no shift of Ti peaks position was observed in our study, that is on the other hand evidenced when solid solutions are formed after 1h milling in Ti–C and Ti–B mixtures [30], the latter phenomena may be excluded among the possible causes for graphite disappearance in the XRD patterns shown in Fig. 1. Thus, graphite amorphization and/or C entrapping between Ti grain boundaries are the most likely motivations which are able to justify the experimental observation above.

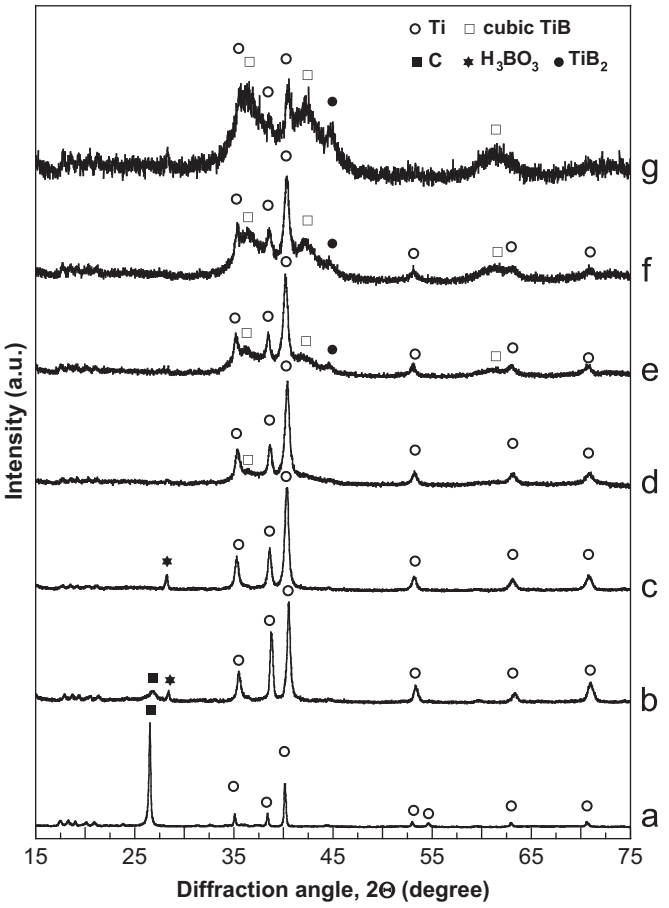

Fig. 1. XRD patterns of Ti–B-C powders as a function of the milling time ($CR = 8$): (a) unmilled, (b) $t_M = 1$h, (c) $t_M = 3$h, (d) $t_M = 6$h, (e) $t_M = 7$h, (f) $t_M = 8$h and (g) $t_M = 12$ h.

Although the mechanical treatment is performed under Ar environment, the formation of H_3BO_3 (boric acid) after 1 h milling is evidenced by the small peak appearing in the XRD pattern, and is possibly caused by moisture adsorbed on the particle surface.

The main change observed in Fig. 1 in the 3 h-6 h milling time range relates to Ti peaks broadening, as a result of grain size refinement and internal strain increase. In particular, the Williamson-Hall method provides an average grain size for Ti of about 250 nm when powders are milled for 6 h. Moreover, this milling time interval also corresponds to the presence of cubic TiB as the first new phase evidenced by XRD, as well as H_3BO_3 peak disappearance.

The incipient formation of one of the two constituent phases of the final composite, namely TiB_2, was observed after 7 h milling treatment at CR = 8 and is accompanied by a relative increase of the amount of Ti monoboride. As the milling time is augmented to 12 h, the peaks intensities

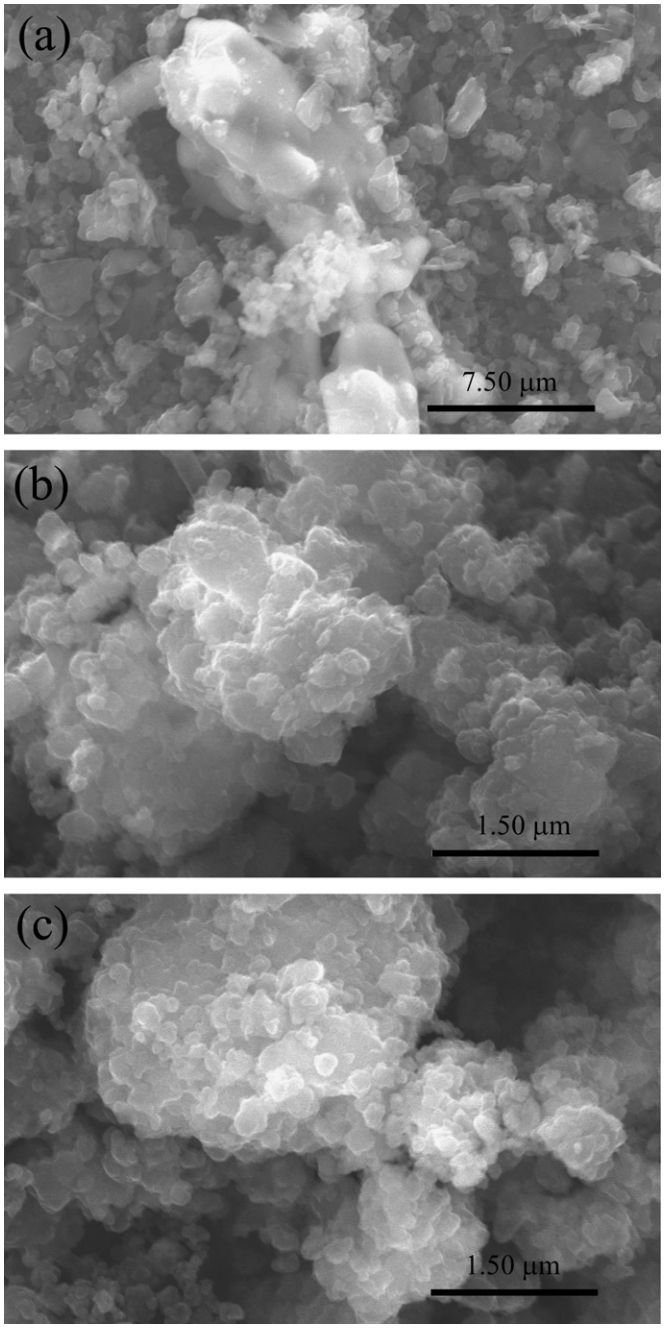

Fig. 2. SEM images of (a) unmilled; (b) 3 h milled and (c) 8 h milled (Ti+6B+C) powders.

of these two boride phases progressively increase, while Ti content correspondingly decreases. Moreover, the indication of marked crystallite refinement and internal strain increase is provided by the significant peaks broadening of reactants and products formed during milling. Unfortunately, the use of the Williamson-Hall formula for estimating crystallites size evolution during milling is not appropriate for time intervals longer than 6 h due to the overlap of the various peaks in XRD spectra (cf. Fig. 1).

Changes in powders characteristics during the milling treatment was also investigated by SEM. Figs. 2**(a)–(c)** show three secondary electron images relative to unmilled, 3 h milled and 8 h milled powders, respectively. Specifically, our analysis was mainly focused on Ti particles, whose size, as mentioned in the Experimental section, was originally larger as compared to B and graphite reactants. It is clearly seen that, the unmilled Ti particles, about 10 μm sized (cf. Fig. 2**a**), are progressively converted into agglomerated consisting of fine grains with sizes falling in the nanometer range (50–150 nm) for milling time of 8 h (cf. Fig. 2**c**). These values are consistent to the grains size estimate (about 250 nm) obtained by means of the Williamson and Hall method when considering 6h milled powders.

Iron contamination during ball milling was retained at sufficiently low levels, i.e. 0.30 ± 0.3 wt.% and 0.51 ± 0.3 wt%, for the case of 3 h and 8 h milled samples, respectively.

The contamination from Fe, WC and other metals (about 2 wt%) was observed during milling of B_4C and TiB_2 powders using WC based milling media [10]. As mentioned in the introduction, WC contamination was also evidenced by XRD in the literature [17], where the milling of Ti, B and C powders was investigated. Both studies reported that (Ti, M)B_2 solid solutions (M=W, Fe, etc.) were formed during the subsequent sintering step. In this regard, no evidence of similar phases was found in the present work, likely due to the relatively low contamination level obtained.

3.2. Reactive spark plasma sintering

3.2.1. Unmilled powders

3.2.1.1. Effect of sintering time. Simply blended Ti, B and graphite powders combined in stoichiometric proportions according to reaction (1) were first considered. The sample displacement (shrinkage) and temperature time profiles measured during the synthesis and simultaneous consolidation process when $I=1100$ A and $P=20$ MPa are shown in Fig. 3 for the case of unmilled powders.

No significant changes in the δ parameter are observed for time intervals shorter than 225 s which correspond to temperature levels lower than about 1040 °C. Subsequently, a gradual increase of sample shrinkage up to about 0.3 mm takes place between 225 and 250 s, while it remains approximately constant until a temperature of about 1370 °C is achieved (290 s). Afterwards, δ progressively increases until its maximum value of about 2.3 mm is reached at the end of the experiment (600 s), when the measured temperature was about 1710 °C.

The mechanism of formation and the densification behavior of the B_4C–TiB_2 composite during the reactive SPS process was then investigated under the same electric current intensity ($I=1100$ A) and applied pressure ($P=20$ MPa), for different time intervals ranging from $t_0=0$ (starting powders) to $t_f=600$ s (final product), as indicated in Fig. 3.

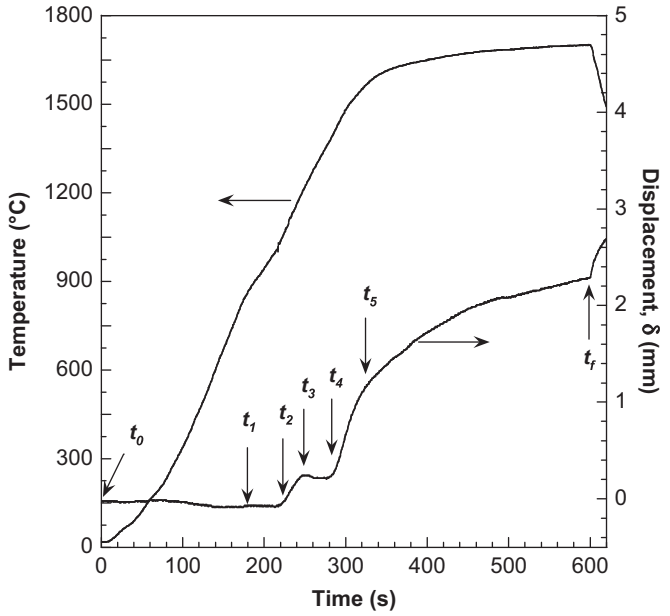

Fig. 3. Sample displacement- and temperature–time profiles during reactive SPS (I=1100 A, P=20 MPa) for the case of unmilled powder.

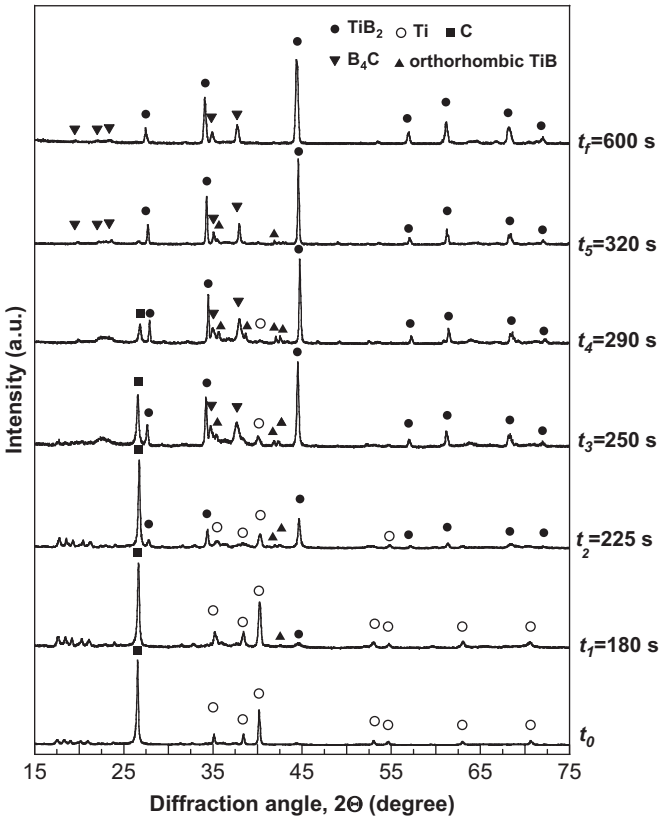

Fig. 4. XRD patterns of final products obtained by reactive SPS starting from (Ti+6B+C) unmilled powders for different values of the time interval (cf. Fig. 3) during which the pulsed electric current is applied (I=1100 A, P=20 MPa).

The compositional changes of the Ti–B–C system for the case of unmilled powders may be then seen in Fig. 4, where the XRD patterns of the corresponding products are reported. The incipient formation of TiB_2 is observed after approximately t_1=180 s when the recorded temperature is about 870 °C, while only reactants were found for the case of shorter time intervals. Traces of the orthorhombic TiB phase are also detected by XRD at t_1. This outcome is consistent with literature results, where the formation during SPS of TiB and TiB_2 from a (Ti+B) mixture was reported to start above 700 °C [32]. It is expected that the chemical interaction of Ti and B leads first to the formation of Ti monoboride (Ti+B→TiB) that is subsequently converted to TiB_2 (TiB+B→TiB_2).

As the sintering time is prolonged to t_2=225 s (T=1040 °C), the intensity of TiB_2 peaks increases and the presence of TiB in the product is confirmed, while the height of Ti peaks remarkably decrease. It should be noted that no melting phases are formed up to this stage, as evidenced by the absence of displacement variation during this time interval (cf. Fig. 3). Thus, consistently to the relatively low temperature level achieved at this stage, product formation takes place through a solid-state mechanism. The rapid increase of the diboride phase amount observed when t_3=250 s (T=1220 °C), is accompanied by the first evidence of B_4C formation and the corresponding decrease of graphite peak (B+4C→B_4C). This finding is in good agreement with previous literature studies where the formation of boron carbide from amorphous boron and carbon black was reported to occur at about 1200 °C during SPS [33].

No additional phases are apparently formed in the time interval t_3-t_4 (250–290 s), although Ti peaks drop out and graphite content markedly decreases, as an indication of the progress of synthesis reactions. As the sample temperature approaches the value of about 1570 °C (t_5=320 s), TiB_2 and B_4C are basically the only significant phases detected in the obtained product, while both residual graphite and TiB tend to disappear from XRD spectra. Therefore, the synthesis reaction can be considered completed at about 1600 °C, since only slight differences in product composition are evidenced by XRD, as the current application is prolonged to t_f.

Other than producing the desired composition of the ceramic composite, the further important goal is the achievement of highly dense products. Thus, the influence of the time interval during which the pulsed current (I=1100 A) is applied on the SPSed sample density was also correspondingly monitored. As reported in Fig. 5, the densification behavior is qualitatively similar to that of the displacement output (cf. Fig. 3), thus indicating that the contribution from thermal expansion in not relevant in this case. This consideration holds also true when examining the milled systems taken into account in next sections. It is confirmed that sample densification becomes significant only for sintering times longer than t_4 and temperatures higher than 1370 °C, i.e. when the reactants are almost completely converted to the desired ceramic phases. Thus,

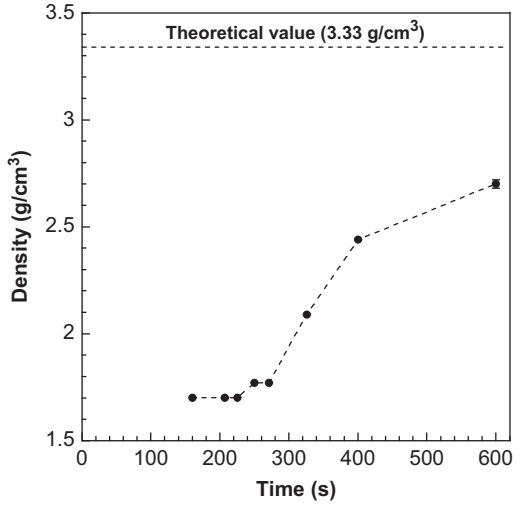

Fig. 5. Density of final products obtained by reactive SPS starting from unmilled (Ti+6B+C) powders for different values of the time interval during which the pulsed electric current is applied (I=1100 A, P=20 MPa).

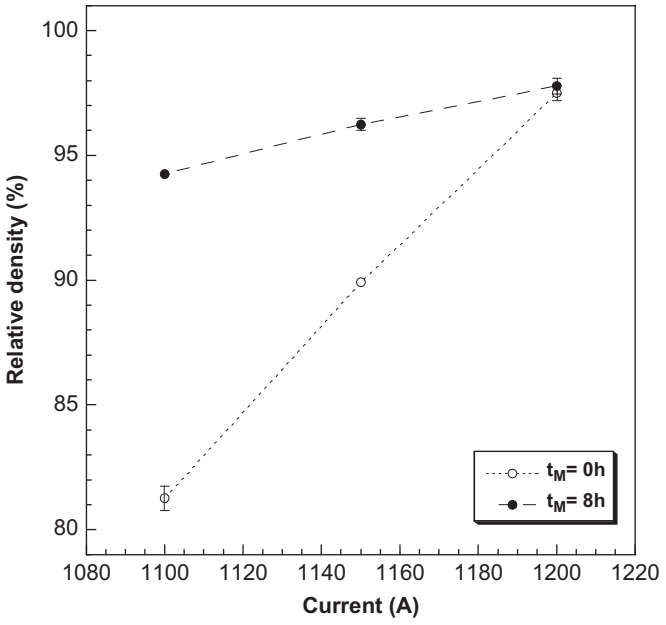

Fig. 6. Effect of applied electric current on the relative density of final products obtained by reactive SPS starting from unmilled and 8h ball milled (Ti+6B+C) powders (P=20 MPa, t_T=10 min).

the refractory character of the TiB_2 and B_4C formed makes product densification difficult so that a rather porous composite material (relative density of about 81.3%) is obtained at the end of the experiment (t_f=600 s, T=1710 °C) under the adopted current/temperature conditions.

3.2.1.2. Effect of current level. In order to improve product density, the influence of the pulsed electric current intensity on the simultaneous synthesis and densification of the TiB_2–B_4C composite was then investigated in the range of 1100–1200 A, while mechanical pressure and sintering time were maintained constant at 20 MPa and 10 min, respectively. From the obtained results reported in Fig. 6 for both the unmilled and 8h milled systems, it can be seen that higher current levels lead to significantly denser composites. Specifically, a near to fully dense material (97.5% relative density) is produced when the applied current to sinter the unmilled powders is increased to 1200 A. Correspondingly, the maximum temperature recorded was about 1820 °C.

This result was confirmed by SEM investigation. In this regard, Figs. 7**(a) and (b)** show two back-scattered micrographs relative to products obtained when I=1100 and 1200 A, respectively. The two TiB_2 (lighter) and B_4C (darker) phases synthesized during reactive sintering are easily distinguishable. It is also clearly seen that the residual porosity present in the sample sintered at the lower current level is markedly reduced when increasing its intensity to 1200 A.

This outcome can be readily justified on the basis of the increased electrical power supplied to the system undergoing sintering when the intensity of the applied current is augmented. Indeed, the correspondingly higher temperature levels and heating rates achieved by Joule effect promote sintering phenomena among powders, thus improving sample densification. The XRD analyses of SPSed samples

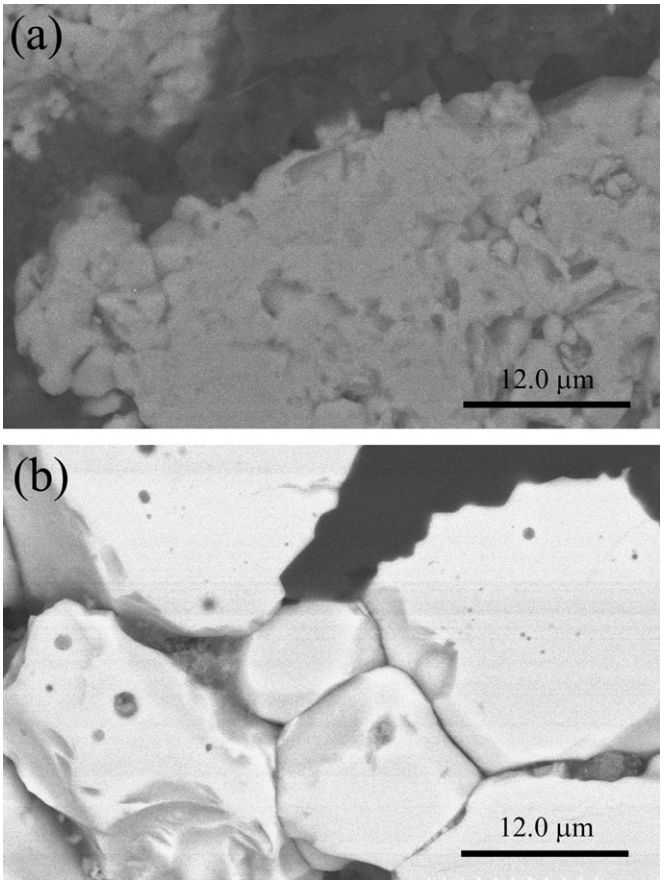

Fig. 7. SEM micrographs of final products obtained by reactive SPS starting from unmilled (Ti+6B+C) powders (P=20 MPa, t_T=10 min): (a) I=1100 A, (b) I=1200 A.

as a function of the applied current, not shown here for the sake of brevity, do not exhibit noteworthy changes in product composition, while TiB_2 and B_4C peaks become more intense and narrow. This fact can be associated to the grain growth favored by the higher sintering temperature reached when the current intensity is increased.

3.2.2. Milled powders

3.2.2.1. Effect of the sintering time

After the optimal sintering conditions for obtaining the near fully dense B_4C–TiB_2 composite from as-received powders have been identified, the effect of the milling treatment on the SPS process dynamics, reactants conversion, relative density, and product microstructure is systematically investigated, as reported in what follows. In particular, the results obtained for the case of (Ti+6B+C) powders co-milled for 3 and 8 h at CR=8 will be analyzed in detail. For the sake of comparison, the milled powders were first processed in the SPS apparatus under the same operating conditions (I=1100 A, P=20 MPa) adopted in the previous section relatively to unmilled powders.

The sample shrinkage profile recorded during the reactive SPS process of 3 h co-milled powders is reported in Fig. 8. With respect to the sintering of unmilled powders (cf. Fig. 3), it was found that milling did not give rise to a significant variation of the obtained temperature profiles, so that the corresponding plot is not shown in this case. On the other hand, some differences are displayed by the displacement behavior.

The evolution of product composition and density during the reacting sintering process of milled powders was then monitored by following the same strategy adopted for as received powders. Thus, a series of specimens to be characterized from the compositional and density points of view are produced by interrupting the application of the electric current at the different time intervals t_i, in the range of 0–10 min, as indicated in Fig. 8. The corresponding XRD patterns are reported in Fig. 9. As described in section 3.1, the XRD analysis of 3 h co-milled powders did not reveal any additional phase formed during the mechanical treatment, with the only exception of a small peak of H_3BO_3, due to the moisture/oxygen present in original boron powders.

The increase of about 0.3 mm in the sample displacement occurring after about 50 s from the application of the current does not correspond to the appearance of new phases in the products undergoing sintering. However, a slight gas evolution took place during this time interval, as manifested by the corresponding increase of the gas pressure inside the SPS chamber. Based on this feature, the change in sample shrinkage is likely associated to H_3BO_3 vaporization, as confirmed by the related peak decrease in the XRD performed when t_1=100 s (320 °C). As the experiment proceeds thus reaching about 620 °C (t_2=140 s), cubic TiB was also detected as a new phase in the XRD spectra. However, Ti peaks appear broaden and

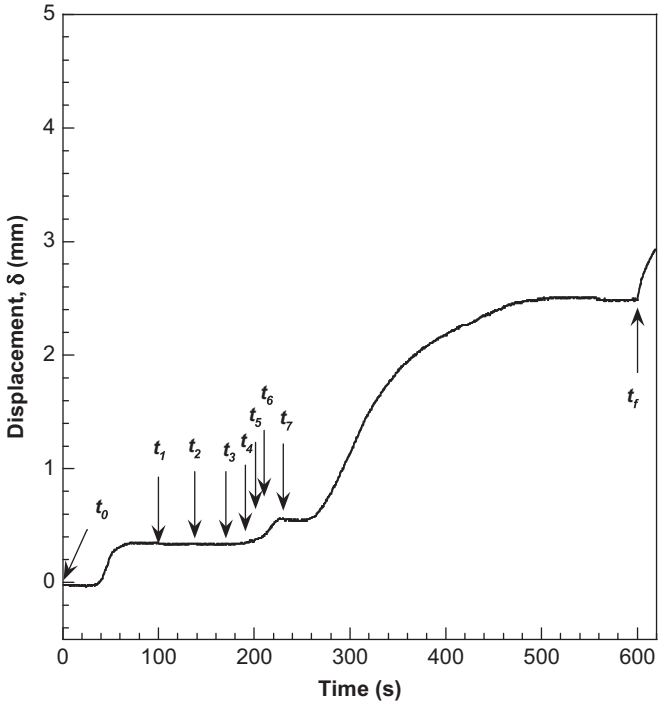

Fig. 8. Sample displacement-time profiles during reactive SPS (I=1100 A, P=20 MPa) for the case of 3 h ball milled (Ti+6B+C) powders.

left-shifted in their position as a consequence of boron diffusion within Ti structure to form a Ti–B solid solution. Thus, in comparison with the case of unmilled powders, the appearance of TiB during reactive sintering seems to be slightly anticipated as a consequence of the milling treatment. On the other hand, similarly to the behavior displayed by as received reactants, the first evidence of the TiB_2 formation was found when T is equal to about 800 °C (t_3=170 s). Moreover, while the presence of TiB is partially hidden by Ti peaks broadening, another phase, that seems to correspond to an unknown species found during a recent investigation involving the reactive sintering of B_4C-23 vol% TiB_2 [17], is also evidenced in the XRD pattern (2θ of about 37.5°). Product composition changes significantly only 20 s later (t_4=190 s), when the measured temperature is about 890 °C. Indeed, TiB_2 becomes the main phase in the product, while the intensity of Ti peaks strongly decreases and small amounts of TiB (cubic and orthorhombic structures) are also found along with some traces of the unidentified phase. It should be noted that the latter one behaves like an intermediate phase since it tends to disappear, as well as the residual Ti, when t_5=200s (T=930 °C). Orthorhombic and cubic TiB (minor amounts) are still detected in the product. However, as the temperature level was increased to about 1000 °C (t_6=210s), they are completely converted to TiB_2, which is the only crystalline phase revealed by XRD at this stage. It is clearly seen that the chemical transformations taking place during the time interval t_1-t_6 do not correspond to any change in the δ parameter.

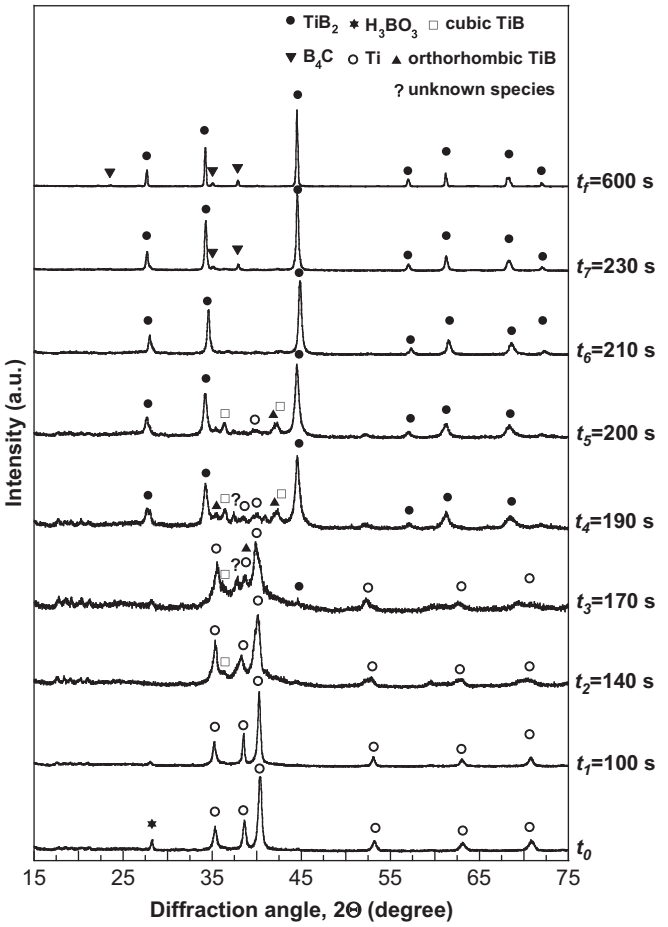

Fig. 9. XRD patterns of final products obtained by reactive SPS starting from 3 h ball milled (Ti+6B+C) powders for different values of the time interval (cf. Fig. 8) during which the pulsed electric current is applied (I=1100 A, P=20 MPa).

As the SPS process proceeds up to t_7=230s and the corresponding measured temperature is of about 1100 °C, the XRD analysis evidences the occurrence of B_4C formation. This event is accompanied by a small increase in the sample displacement (cf. Fig. 8). Finally, no changes from the compositional point of view are found until the end of the sintering experiment (t_f=600 s). On the basis of the obtained results, the reaction for the synthesis of B_4C–TiB_2 composite goes to completion at lower temperature levels when starting from 3 h milled powders ($\leq$ 1100 °C) as compared to the case of as-received reactants (about 1600 °C). This is an unequivocal indication of the importance of interface formation between reactants induced by ball milling to promote diffusion phenomena, and consequent chemical transformations, during reactive SPS.

As far as the densification behavior is concerned, at the time interval when the reaction can be considered completed (about 230 s), it is found that the obtained material is still extremely porous, being its relative density slightly above 60%. Thus, higher temperatures and prolonged sintering times are required to achieve adequate densification levels. Specifically, a 97% dense composite material is produced at the end of the SPS process. This is an important achievement, which demonstrates the marked effect of the 3h milling treatment to improve powders densification, as compared to the best result obtained under the same sintering conditions while processing simply blended reactants (cf. Fig. 5).

A back-scattered SEM image of the fully dense specimen produced when using 3h milled powders is reported in Fig. 10. Sample microstructure appears in this case significantly different from that found for unmilled powders (cf. Fig. 7).

A significant TiB_2 grain size refinement is evidenced in Fig. 10 in comparison with the situation displayed in Fig. 7**(b)** relatively to unmilled powders, thus manifesting an important effect of the milling treatment on the microstructural characteristics of the bulk composite material. However, a rather wide grains size distribution is obtained and the produced TiB_2 (lighter) and B_4C (darker) phases are not homogeneously dispersed throughout the sample. This fact is likely ascribed to the heterogeneous nature of the ball milling treatment, which may provide, unless prolonged milling times are adopted, powders to be sintered with different characteristics (grain size, reactivity, etc.).

Let us now consider the reactive sintering of 8 h milled powders. The sample displacement temporal changes correspondingly recorded when the applied current was equal to 1100 A are shown in Fig. 11. Also in this case, the temperature time profile is not reported here since it provides similar values to that recorded when as-received powders were processed under the same SPS conditions (cf. Fig. 3).

Differently from the unmilled and 3 h milled systems examined previously, Fig. 11 indicates that the 8h milled sample shrinkage is almost exclusively confined to the sintering time interval of 220–340 s, corresponding to a temperature range of about 1000–1600 °C. Thus, as compared to less severely milled powders, displacement

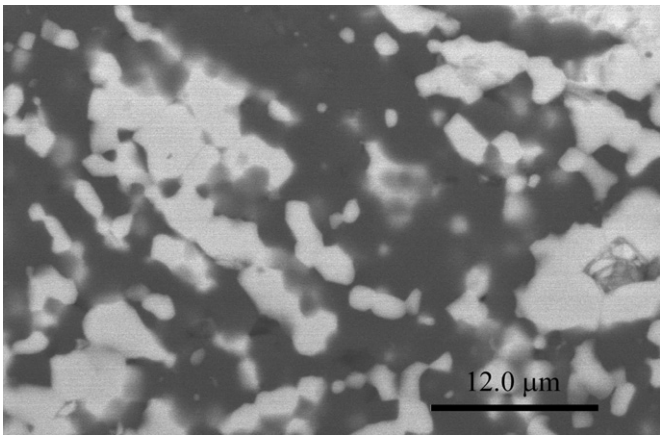

Fig. 10. SEM micrograph (2500x) of the end product obtained by reactive SPS starting from (Ti+6B+C) 3h milled powders (I=1100 A, P=20 MPa, t_T=10 min).

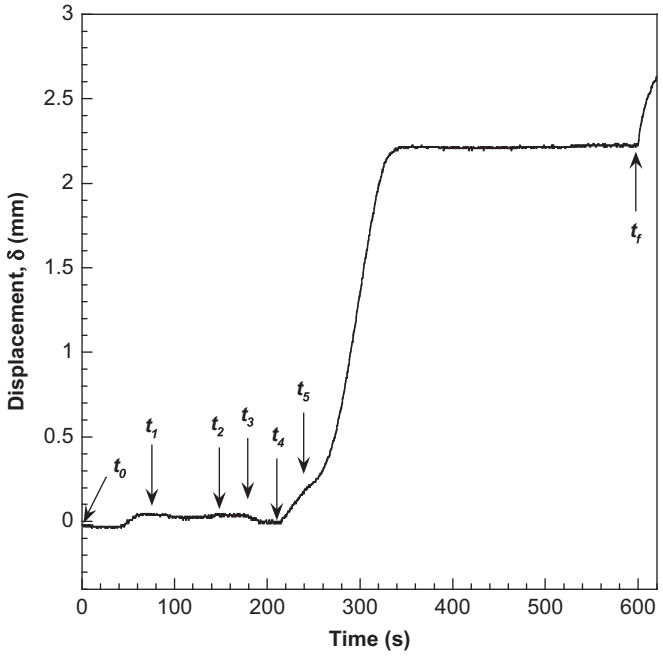

Fig. 11. Sample displacement-time profiles during reactive SPS (I=1100 A, P=20 MPa) for the case of 8 h co-milled powders.

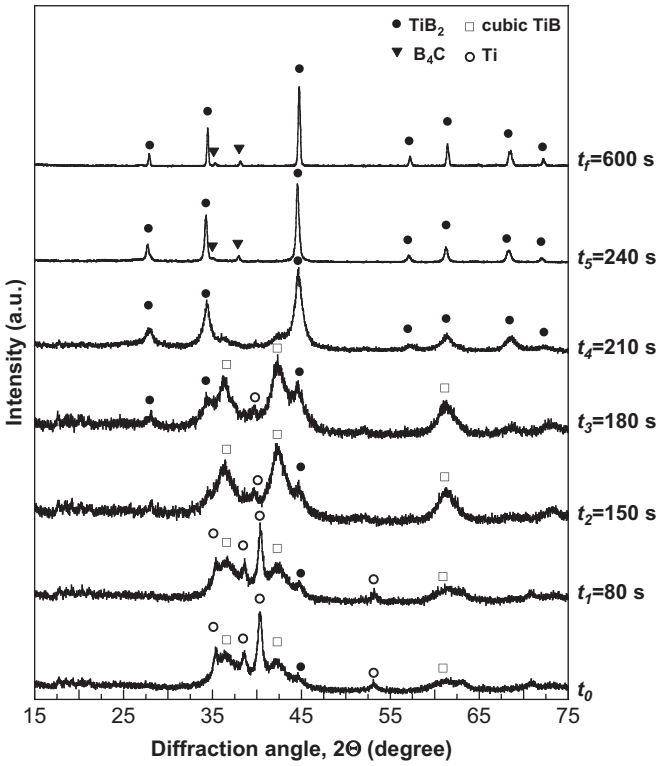

Fig. 12. XRD patterns of final products obtained by reactive SPS starting from 8 h milled (Ti+6B+C) powders for different values of the time interval (cf. Fig. 11) during which the pulsed electric current is applied (I=1100 A, P=20 MPa).

changes take place at a relatively higher rate and the final value of δ (about 2.3 mm) is reached sooner.

The evolution of chemical composition during the synthesis process is shown in Fig. 12. In this case, the powders undergoing sintering (t_0=0 s) initially contain certain amounts of TiB_2 and TiB formed during milling. No compositional transformations are evidenced by XRD analysis at t_1=80 s (290 °C). However, when the reactive process was interrupted at t_2=150 s, although the corresponding thermal levels are rather low (T=690 °C), a significant conversion of Ti to TiB is observed, while the TiB_2 content modestly increases. This outcome indicates the improved reactivity of the powders mixture to induce B diffusion into Ti matrix to form TiB (Ti+B→TiB) as a consequence of the relatively intense mechanochemical activation received. As the temperatures was increased to about 860 °C (t_3=180 s), the XRD analysis reveals a slight TiB_2 increase at the expenses of TiB. Nevertheless, product composition changes completely 30 s later (t_4=210 s, T=1000 °C), when the most relevant crystalline phase detected in the sample is TiB_2 with only traces of TiB. It should be noted that the significant peaks broadening of the diboride phase indicates that the corresponding crystallites are maintained relatively fine. Indeed, the application of the Williamson-Hall method at this sintering stage provides an average crystallite size of TiB_2 lower than 50 nm.

The synthesis of B_4C was evidenced at about 1180 °C (t_5=240 s), while the sample displacement shows only a modest increase. A significant TiB_2 peaks narrowing is correspondingly observed, thus denoting grain growth occurrence. Nevertheless, an average crystallite size lower than 100 nm was estimated using the Williamson-Hall formula. This holds also true as the sintering process proceeds until the end of the experiment.

According to the sample displacement output reported in Fig. 11, density measurements of SPSed products obtained from the 8 h milled powders still evidence that the most relevant powder consolidation follows reaction completion. Indeed, while extremely porous samples are obtained at the time interval when the original reactants and intermediate phases are fully converted to TiB_2 and B_4C, material porosity is rapidly reduced as the temperature levels increase. However, despite of the plateau observed in the displacement curve (cf. Fig. 11), the complete densification of the composite product was not achieved when applying this current level (1100 A), being the maximum relative density obtained equal to about 94.3%.

The data related to the influence of milling time on the density of end-products obtained by reactive SPS under the same sintering conditions, i.e. I=1100 A, P=20 MPa, t_T=10 min, are summarized in Fig. 13. As milling time is augmented, the density first increases significantly, reaches a maximum when using 3 h milled powders, and then gradually decreases. Such behavior is similar to that observed when investigating the reactive sintering by SPS of TiC–TiB_2 composites using mechanically activated Ti, B_4C, and C reactants [34] and can be justified as follows. As milling process proceeds, powders size decreases and

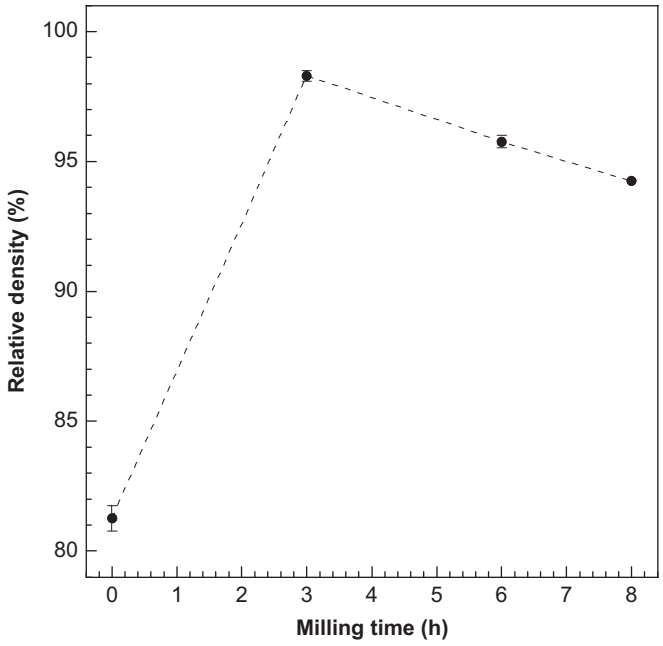

Fig. 13. Effect of milling time on the relative density of the bulk samples obtained at the same SPS conditions (I=1100A, P=20 MPa, t_T=10 min).

interfacial formation between reactants is progressively promoted. Both these features facilitate mass transport by diffusion and, therefore, the occurrence of synthesis and sintering phenomena. On the other hand, the refractory nature of products formed during the mechanical treatment, in particular TiB and TiB_2 in our system, may hinder powder densification, thus leading to residual porosity in final bulk products. This explanation is in agreement with the XRD analysis results of the differently milled powders reported in Fig. 1. Indeed, no product is formed after 3 h milling while significant amounts of TiB and TiB_2 are found when the treatment is prolonged to 8 h. Thus, a fully dense product is obtained at 3 h milling time while this condition is not satisfied when such treatment is prolonged. Consistently, the intermediate behavior displayed by 6 h milled powders indicates that the incipient formation of ceramic products, i.e. TiB along with the other possible minor refractory phases whose amounts are present below the detection limit of XRD analysis, starts to play a role in this regard.

Another possible reason to justify the observed densification behavior relates to the tendency of nanocrystalline particles to agglomerate, that is well known to negatively affect powder densification [35–37]. Indeed, as seen in Figs. 2**(a)–(c)**, the milling treatment gives rise to the formation of large agglomerates of fine grains. Thus, it is likely that for milling times longer than 3 h, such phenomenon may hinder powder consolidation, thus contributing to explain the relative density decreasing observed in Fig. 13.

3.2.2.2. *Effect of current*

Since prolonged milling treatments are found to produce relatively difficult-to-sinter powders, higher current levels are required to improve SPSed product density. Thus, analogously to the simply blended powders, the electric current intensity was increased in the range of 1100–1200 A, while maintaining constant the other sintering conditions. The obtained data shown in Fig. 6 along with the results related to the unmilled system indicate that the application of 1150 A provides a product with relative density higher than 96% while an almost 98% dense sample is produced at 1200 A.

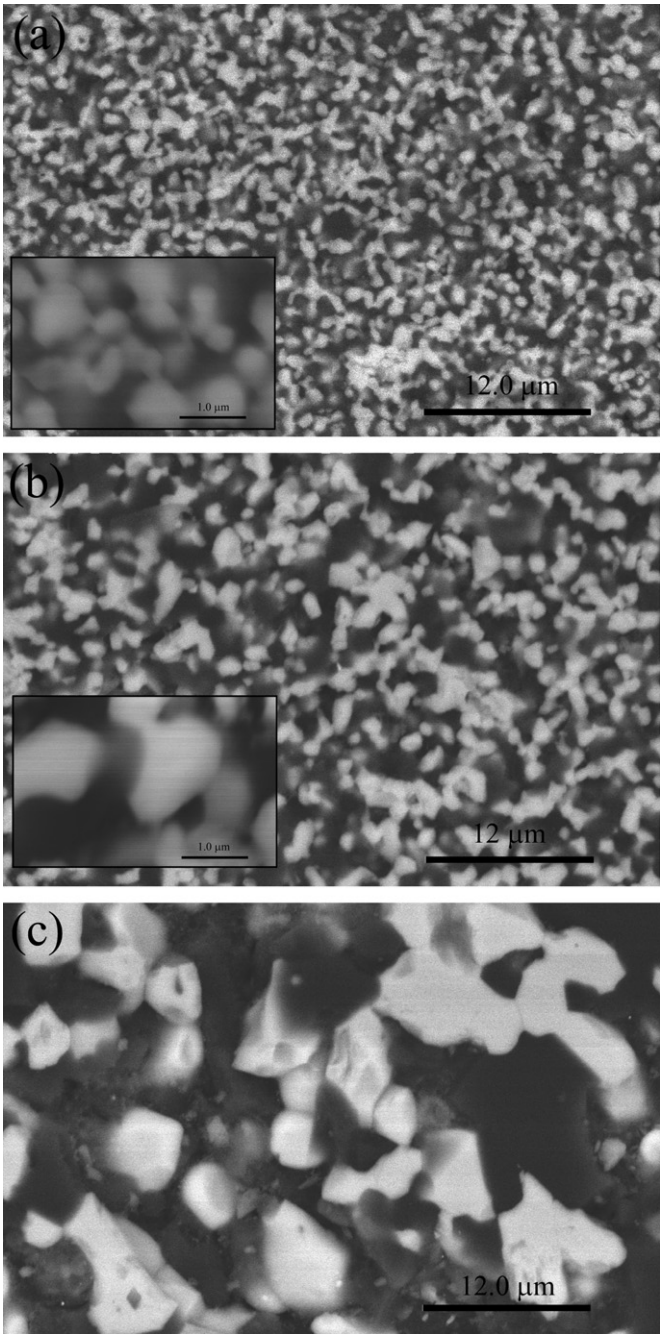

Fig. 14. SEM micrographs of final products obtained by reactive SPS starting from 8 h ball milled (Ti+6B+C) powders (P=20 MPa, t_T=10 min): (a) I=1100 A, (b) I=1150 A and (c) I=1200 A.

The microstructures of corresponding composite materials are compared in Figs. 14**(a)–(c),** where three SEM back scattered images related to the different electric current conditions are reported. A very homogeneous and fine grained microstructure is obtained at 1100 A, if compared to the results previously described and related to original (cf. Fig. 7) or milder-milled (cf. Fig. 10) powders sintered under the same current conditions. In particular, grains size of both ceramic phases is on the order of 1 μm or less (cf. see inset of Fig. 14**(a)**), thus indicating the beneficial influence of the mechanical treatment to the obtainment of massive fine-grained TiB_2–B_4C composites. Such accomplishment could be associated to the fact that ball milling promotes an increase in the nucleation rate of product phases as compared to the grain growth. Along this direction, the prominent role is played by the combined effect of reactants/products grain refinement, the interface formation between reagents as well as the presence of the TiB and TiB_2 phases formed during ball milling, that act as crystallization seeds during the synthesis process by SPS.

As the applied current is augmented to 1150 A (cf. Fig. 14**(b)**), a good homogeneity in phases distribution is maintained while the grains size of TiB_2 and B_4C are found to increase only slightly (1–2 μm) as compared to the case displayed in Fig. 14**(a)**.

On the other hand, a significantly coarser grained microstructure is obtained when the 8 h milled powders were sintered at 1200 A (cf. Fig. 14**(c)**) thus indicating that the improvement of product densification at higher currents occurred in this case at the expenses of a marked grain growth.

On the basis of the results described above, it is possible to state that, when using 8 h milled elemental powders, the most preferable current intensities to be adopted by reactive SPS for obtaining a nearly full dense TiB_2–B_4C composite with very fine and uniform microstructure are in the range of 1100–1150 A, while higher values produce excessive grain growth.

4. Concluding remarks

The combined effect of mechanical and electric current activation on the simultaneous synthesis and densification of B_4C–TiB_2 composite was investigated. Specifically, Ti, B and graphite powder reactants are first preliminarily co-milled at different time intervals and then reactively sintered using a SPS apparatus.

Sintering time and electric current level are found to strongly affect the composition and density of the obtained bulk material. In particular, when using unmilled powders, a near fully dense composite (about 97% relative density), only consisting of TiB_2 and B_4C phases and characterized by relatively coarse microstructure**,** was obtained under the optimal SPS time (10 min total) and current level (1200 A).

The mechanical treatment of starting reactants was found to promote grain size refinement (up to 50–150 nm) and, for milling times longer than 6 h (CR = 8), the formation of TiB and TiB_2, while B_4C was not detected in the processing powders even when the more intense milling conditions (12 h) were adopted.

Some insights on the mechanism of formation of the ceramic composite are provided by analyzing the SPS products resulting after the interruption of the synthesis process at different time intervals. It was found that the intermediate TiB compound is the first phase formed as a consequence of Ti boriding. However, as the SPS holding time is increased, the monoboride phase is gradually converted to TiB_2 while the formation of B_4C required the achievement of higher temperature level.

The milling treatment was found to markedly affect the conditions needed for the complete reactants conversion. For instance, residual graphite and TiB are still found at 1430 °C when starting from unmilled powders, while only the two desired phases are present in SPSed samples at 1100 °C when using 3 h or 8 h milled powders.

Furthermore, on the basis of the relatively low temperature levels recorded during the entire synthesis process, it is possible to state that all transformations during reactive SPS of the B_4C–TiB_2 composite are governed by a solid-state diffusion mechanism.

Product density obtained by SPS when I = 1100 A was observed to increase from about 82% to 97% of the theoretical value, when the original powders were milled for 3 h, while further increase of the milling time led to a density decrease down to about 94.3% for the 8 h milled system. On the other hand, the latter conditions also correspond to the material with the finer microstructure (on the order of 1 μm or less) and homogeneous phase distribution. An increase of the applied current intensity to 1150 A allows for the improvement of product density (higher than 96%) at the expenses of a slight microstructure coarsening. Nevertheless, the improvement in product densification when the current is further augmented is accompanied by a remarkable grain growth of both composite constituents.

Acknowledgments

One of us (L.N.) acknowledges the University of Cagliari (Italy) for the six-month period spent at the Dipartimento di Ingegneria Meccanica, Chimica e dei Materiali during which this work has been performed. The authors thank Dr. Selena Montinaro (University of Cagliari, Italy) for determining iron contamination on milled powders. The company D.N.M. (Dense Nanostructured Materials) S.r.l. (Sestu, Cagliari, Italy) is also acknowledged for granting the use of the SPS 515S model equipment.

References

[1] F. Thevenot, Boron Carbide-Comprehensive Review, Journal of The European Ceramic Society 6 (1990) 205–225.

[2] D.K. Kim, C.H. Kim, Pressureless sintering and microstructural development of B_4C–TiB_2 based composites, Advanced Ceramic Materials 3 (1988) 52–55.
[3] G. Sasaki, T. Suga, T. Yanai, K. Suganuma, K. Niihara, Microstructure of B_4C/TiB_2 composite fabricated by reaction sintering of B_4C and TiC, Journal of the Ceramic Society of Japan 102 (4) (1994) 320–323.
[4] T. Graziani, A. Bellosi, Production and characteristics of B_4C/TiB_2 composites, Key Engineering Materials 104-107 (Pt 1) (1995) 125–132.
[5] L.S. Sigl, H.J. Kleebe, Microcracking in B_4C–TiB_2 composites, Journal of the American Ceramic Society 78 (9) (1995) 2374–2380.
[6] S. Tuffé, J. Dubois, G. Fantozzi, G. Barbier, Densification, Microstructure and mechanical properties of TiB_2–B_4C based composites, International Journal Of Refractory Metals and Hard Materials 14 (1996) 305–310.
[7] H. Itoh, K. Sugiura, H. Iwahara, Preparation of TiB_2–B_4C composites by high pressure sintering, Journal of Alloys and Compounds 232 (1996) 186–191.
[8] L. Levin, N. Frage, M.P. Dariel, Novel approach for the preparation of B_4C-based cermets, International Journal of Refractory Metals and Hard Materials 18 (2) (2000) 131–135.
[9] V. Skorokhod, V.D. Krstic, Processing, microstructure, and mechanical properties of B_4C–TiB_2 particulate sintered composite. Part I: pressureless sintering and microstructural evolution, Powder Metallurgy and Metal Ceramics 39 (2000) 504–512.
[10] K.F. Cai, C.W. Nan, M. Schmuecker, E. Mueller, Microstructure of hot-pressed B_4C–TiB_2 thermoelectric composites, Journal of Alloys and Compounds 350 (1-2) (2003) 313–318.
[11] S. Yamada, K. Hirao, Y. Yamauchi, S. Kanzaki, High strength B_4C–TiB_2 composites fabricated by reaction hot-pressing, Journal of The European Ceramic Society 23 (2003) 1123–1130.
[12] J.E. Zorzi, C.A. Perottoni, da Jornada JAH. Hardness and wear resistance of B_4C Ceramics prepared with several additives, Materials Letters 59 (2005) 2932–2935.
[13] T.S. Srivatsan, G. Guruprasad, D. Black, M. Petraroli, R. Radhakrishnan, T.S. Sudarshan, Influence of TiB_2 content on microstructure and hardness of TiB_2–B_4C composite, Powder Technology 159 (2005) 161–167.
[14] H.R. Baharvandi, A.M. Hadian, A. Alizadeh, Processing and mechanical properties of boron carbide–titanium diboride ceramic matrix composites, Applied Composite Materials 13 (3) (2006) 191–198.
[15] A. Goldstein, Y. Yeshurun, A. Goldenberg, B_4C/metal boride composites derived from B_4C/metal oxide mixtures, Journal of The European Ceramic Society 27 (2-3) (2007) 659–700.
[16] I. Bogomol, T. Nishimura, O. Vasylkiv, Y. Sakka, P. Lobodo, Microstructure and high-temperature strength of B_4C–TiB_2 composite prepared by a crucibleless zone melting method, Journal of Alloys and Compounds 485 (1-2) (2009) 677–681.
[17] D.V. Dudina, D.M. Hulbert, D. Jiang, C. Unuvar, S.J. Cytron, A.K. Mukherjee, In situ boron carbide–titanium diboride composites prepared by mechanical milling and subsequent Spark Plasma Sintering, Journal of Materials Science 43 (2008) 3569–3576.
[18] X. Yue, S. Zhao, P. Lü, Q. Chang, H. Ru, Synthesis and properties of hot pressed B_4C–TiB_2 ceramic composite, Materials Science and Engineering A 527 (27-28) (2010) 7215–7219.
[19] S.G. Huang, K. Vanmeensel, O.J.A. Malek, O. Van der Biest, Microstructure and mechanical properties of pulsed electric current sintered B_4C–TiB_2 composite, Materials Science and Engineering A 528 (2011) 1302–1309.
[20] S.G. Huang, K. Vanmeensel, O. Van der Biest, J. Vleugels, In situ synthesis and densification of submicrometer–grained B_4C–TiB_2 Composite by pulsed electric current, Journal Of The European Ceramic Society 31 (2011) 637–644.
[21] C. Xu, Y. Cai, K. Flodström, Z. Li, S. Esmaeilzadeh, G.J. Zhang, Spark plasma sintering of B_4C ceramics: the effects of milling medium and TiB_2 addition, International Journal of Refractory Metals and Hard Materials 30 (1) (2012) 139–144.
[22] R. Orrù, R. Licheri, A.M. Locci, A. Cincotti, G. Cao, Consolidation/synthesis of materials by electric current activated/assisted sintering, Materials Science and Engineering R 63 (4–6) (2009) 127–287.
[23] F.L. Matthews, R. Rawlings, Composite Materials: Engineering and Science, Chapman & Hall, Great Britain, 1994.
[24] CRC Materials science and engineering handbook, 3rd ed., CRC Press LLC, 2001.
[25] A.M. Locci, R. Orrù, G. Cao, Z.A. Munir, Simultaneous Spark Plasma Synthesis and Densification of TiC–TiB_2 Composites, Journal of the American Ceramic Society 89 (3) (2006) 848–855.
[26] G.K. Williamson, W.H. Hall, X-ray line broadening from filed aluminium and wolfram, Acta Metallurgica 1 (1953) 22–31.
[27] L.L. Ye, M.X. Quan, Synthesis of nanocrystalline TiC powders by mechanical alloying, Nanostructured Materials 5 (1995) 25–31.
[28] N.Q. Wu, S. Lin, J.M. Wu, Z.Z. Li, Mechanosynthesis mechanism of TiC powders, Journal of Materials Science and Technology 14 (1998) 287–291.
[29] A.S. Ramos, S.P. Taguchi, E.C.T. Ramos, V.L. Arantes, S. Ribeiro, High-energy ball milling of powder B–C mixtures, Materials Science and Engineering A 422 (2006) 184–188.
[30] J. Schmidt, M. Boehling, U. Burkhardt, Y. Grin, Preparation of titanium diboride TiB_2 by spark plasma sintering at slow heating rate, Science and Technology of Advanced Materials 8 (2007) 376–382.
[31] W. Tang, Z. Zheng, Y. Wu, J. Wang, J. Lu, J. Liu, Synthesis of TiB_2 nanocrystalline powder by mechanical alloying, Transactions of the Nonferrous Metals Society of China 16 (2006) 613–617.
[32] B.H. Lohse, A. Calka, D. Wexler, Synthesis of TiC by controlled ball milling of titanium and carbon, Journal of Materials Science 42 (2007) 669–675.
[33] B. Ghosh, S.K. Pradhan, Microstructure characterization of nanocrystalline TiC synthesized by mechanical alloying, Materials Chemistry and Physics 120 (2010) 537–545.
[34] U. Anselmi-Tamburini, Z.A. Munir, Y. Kodera, T. Imai, M. Ohyanagi, Influence of synthesis temperature on the defect structure of boron carbide: experimental and modeling studies, Journal of the American Ceramic Society 88 (2005) 1382–1387.
[35] A. Locci, R. Orrù, G. Cao, Z.A. Munir, Effect of ball milling on simultaneous spark plasma synthesis and densification of TiC-TiB_2 composites, Materials Science and Engineering A 434 (2006) 23–29.
[36] M.J. Mayo, Processing of nanocrystalline ceramics from ultrafine particles, International Materials Reviews 41 (1996) 85–115.
[37] J.R.Nanosintering. Groza, Nanostructured Materials 12 (1999) 987–992.